Environmental and Experimental Botany 91 (2013) 74–83

Contents lists available at SciVerse ScienceDirect

Environmental and Experimental Botany

journal homepage: www.elsevier.com/locate/envexpbot

Iron deprivation-induced reactive oxygen species generation leads to non-autolytic PCD in *Brassica napus* leaves

Rajesh Kumar Tewari [a,*], Franz Hadacek [b], Stefan Sassmann [c], Ingeborg Lang [c]

[a] Department of Terrestrial Ecosystem Research (TER), Faculty of Life Sciences, University of Vienna, Althanstrasse 14, 1090 Vienna, Austria
[b] Albrecht-von-Haller Institut, Plant Biochemistry, Georg-August-Universität Göttingen, Justus-von-Liebig-Weg 11, 37077 Göttingen, Germany
[c] Cell Imaging and Ultrastructure Research (CIUS), Faculty of Life Sciences, University of Vienna, Althanstrasse 14, 1090 Vienna, Austria

ARTICLE INFO

Article history:
Received 9 December 2012
Received in revised form 17 February 2013
Accepted 22 March 2013

Keywords:
Brassica napus
Caspase
Iron
Deprivation
Deficiency
Programmed cell death
Reactive oxygen species

ABSTRACT

Using iron-deprived (–Fe) chlorotic as well as green iron-deficient (5 μM Fe) and iron-sufficient supplied (50 μM Fe) leaves of young hydroponically reared *Brassica napus* plants, we explored iron deficiency effects on triggering programmed cell death (PCD) phenomena. Iron deficiency increased superoxide anion but decreased hydroxyl radical (•OH) formation (TBARS levels). Impaired photosystem II efficiency led to hydrogen peroxide accumulation in chloroplasts; NADPH oxidase activity, however, remained on the same level in all treatments. Non-autolytic PCD was observed especially in the chlorotic leaf of iron-deprived plants, to a lesser extent in iron-deficient plants. It correlated with higher DNAse-, alkaline protease- and caspase-3-like activities, DNA fragmentation and chromatin condensation, hydrogen peroxide accumulation and higher superoxide dismutase activity. A significant decrease in catalase activity together with rising levels of dehydroascorbic acid indicated a strong disturbance of the redox homeostasis, which, however, was not caused by •OH formation in concordance with the fact that iron is required to catalyse the Fenton reaction leading to •OH generation. This study documents the chain of events that contributes to the development of non-autolytic PCD in advanced stages of iron deficiency in *B. napus* leaves.

© 2013 Elsevier B.V. Open access under CC BY-NC-ND license.

1. Introduction

Iron is an essential element for all forms of life, and its limitation has a profound impact on the productivity of photosynthetic organisms (Frey and Reed, 2012; Jeong and Guerinot, 2009). This common transition metal is a co-factor of many proteins that are involved in cellular processes, including respiration, photosynthesis and cell differentiation (Broadley et al., 2012). Iron is required by many antioxidant enzymes as it is an important catalyst of electron transfer reactions. Potential targets comprise reactive oxygen species (ROS), such as H_2O_2 (hydrogen peroxide) and •OH (hydroxyl radical), which are either reduced to H_2O (antioxidant activity), or oxidized, such as $O_2^{\bullet -}$ (superoxide anion radical) with concomitant reduction of Fe^{III} to Fe^{II}. Moreover, the reduction of molecular oxygen to $O_2^{\bullet -}$ is also possible. Ferrous iron, Fe^{II}, catalyses the reduction of H_2O_2 to •OH, one of the most efficient oxidants in nature (Halliwell, 2006). However, iron-deficient plants reportedly show decreased lipid peroxidation levels compared to controls (Iturbe-Ormaetxe et al., 1995; Tewari et al., 2005). Severe iron deficiency does not result in •OH production, which usually causes lipid peroxidation, although H_2O_2, $O_2^{\bullet -}$ and SOD activity increase (Donnini et al., 2011; Iturbe-Ormaetxe et al., 1995; Kumar et al., 2010; Molassiotis et al., 2006; Tewari et al., 2005). Conversely, increased lipid peroxidation in iron-deficient maize leaves (Sun et al., 2007) and common bean root nodules (Abdelmajid et al., 2008) have also been reported.

Processes to remove redundant, aged, or damaged cells in eukaryotic tissues are designated as programmed cell death (PCD); PCD, however, has been recognized also as an important mechanism in cell differentiation and organ development (Greenberg, 1996; Lam, 2008). Mitochondria and chloroplasts represent recognized sources generating ROS that are involved in signalling cell-death. Iron is an integral component of enzyme complexes, which form the electron transport chains in chloroplasts and mitochondria (Connolly and Guerinot, 2002; Lam, 2008). Recently, chloroplastic ROS generation has been suggested to be involved

Abbreviations: APX, ascorbate peroxidase; AA, ascorbic acid; CAT, catalase; DAB, 3,3′-diaminobenzidine; DAPI, 4′,6-diamidino-2-phenylindole dihydrochloride; DNAse, deoxyribonuclease; DHA, dehydroascorbic acid; DTT, 1,4-dithio-DL-threitol; EDTA, ethylenediaminetetraacetic acid; ETR, electron transport rate; ETS, electron transport system; NBT, *p*-nitro-blue tetrazolium chloride; PCD, programmed cell death; POD, peroxidase; SOD, superoxide dismutase; TBARS, thiobarbituric acid reactive substances; Y(II), effective quantum yield.

* Corresponding author at: Department of Terrestrial Ecosystem Research (TER), Faculty of Life Sciences, University of Vienna, Althanstrasse 14, A-1090 Vienna, Austria. Tel.: +43 1 4277 54262; fax: +43 1 4277 9541.
E-mail addresses: rajesh.tewari@univie.ac.at, rktewari_bot@yahoo.com (R.K. Tewari), franz.hadacek@biologie.uni-goettingen.de (F. Hadacek).

0098-8472 © 2013 Elsevier B.V. Open access under CC BY-NC-ND license.
http://dx.doi.org/10.1016/j.envexpbot.2013.03.006

in apoptotic-like protoplast death (Tewari et al., 2012). In plants, autolytic and non-autolytic PCD are differentiated on basis of cell shrinking and cell swelling. Necrotic phenomena are included into non-autolytic PCD, which also occurs during the hypersensitive response to plant pathogens (Reape et al., 2008; van Doorn, 2011). One of the best characterized forms of PCD in animals is apoptosis, which involves activation of a set of highly specific proteolytic enzymes called caspases [cysteine-dependent aspartate-specific proteases (Chichkova et al., 2012)].

Caspase activation is strictly regulated; upstream (initiator) caspases process the precursors of downstream (executioner) caspases to trigger protein fragmentation. Despite absence of caspase orthologous genes in plant genomes, cells undergoing PCD show caspase-like activity (Belenghi et al., 2004). Plants do have metacaspases (cleavage occurs after the basic residues, arginine, R and lysine, K), which are distant relatives of animal caspases that have a pro-cell death cysteine-dependent protease activity. Moreover, plant serine-dependent protease (phytaspase) shares cleavage specificity and a role in PCD analogous to that of animal caspases (Chichkova et al., 2012). In contrast to animal procaspases, plant caspase-like enzymes are generally secreted from healthy cells into the apoplast and only transported back into cytoplasm during PCD execution (Chichkova et al., 2010).

Despite the recognized significance of iron for plant metabolic processes, including maintaining ROS homeostasis, no study yet has addressed explicitly the extent of iron involvement, deprivation versus deficiency, in PCD development in plants. Iron deficiency has been reported to induce PCD in animal models by increasing cytosolic Ca^{2+} concentrations, depletion of energy and annexin expression in mouse erythrocytes (Kempe et al., 2006) and also to activate caspase-3 activity in human Raji cell lines (Koc et al., 2006). Although generation of $O_2^{\bullet -}$ and H_2O_2 (Donnini et al., 2011) and up-regulation of SOD (Molassiotis et al., 2006) have been reported previously in plants under iron deficiency, the correlation and extent of oxidative stress responses with iron deficiency and deprivation have not yet been explored specifically. For the first time, this study focuses on iron in PCD development in plants by comparing hydroponically reared iron-deprived, -deficient and -sufficient *Brassica napus* leaves (rapeseed). Iron supply (tissue levels and accumulation) was monitored in terms of effects on pigments biosynthesis (chlorophyll *a* and *b*, carotenoids) and PSII efficacy. Oxidative stress was explored by $O_2^{\bullet -}$ and H_2O_2 and lipid peroxidation ($^{\bullet}OH$) levels. Antioxidant defences were characterized by ascorbate concentration and NADPH oxidase, superoxide dismutase, catalase and peroxidase-like activities. All these parameters correlated with the development of non-autolytic programmed cell death, which was documented by nuclear condensation, DNA fragmentation and caspase 3-like, alkaline protease-, and DNAase-like activities.

2. Materials and methods

2.1. Chemicals

All non-specifically annotated chemicals were analytical grade and obtained from Sigma–Aldrich (Schnelldorf, Germany). Water had MilliQ quality.

2.2. Plant material

B. napus plants were grown in hydroponic culture in the glasshouse (night and day temperature respectively 20 and 25 °C, relative humidity 50% and light intensity at noon 400 μmol m^{-2} s^{-1}). Initially, plants were grown in full nutrient solution (Tewari et al., 2005): 2.0 mM KNO_3, 2.0 mM $Ca(NO_3)_2$, 1.0 mM $MgSO_4$, 0.67 mM NaH_2PO_4, 0.05 mM NaCl, 0.05 mM Fe_3–EDTA, 5.0 μM $MnSO_4$, 0.5 μM $CuSO_4$, 0.5 μM $ZnSO_4$, 16.5 μM H_3BO_3, 0.1 μM Na_2MoO_4, 0.05 μM $CoSO_4$ and 0.05 μM $NiSO_4$. The pH of the nutrient solution was adjusted to 6.7 ± 0.2 at the time of supply. After a week of transplantation, pots were divided into three groups. Whereas plants in group 3 continued to receive complete nutrient solution (control), those in groups 1 and 2 were supplied with a nutrient solution with no Fe_3–EDTA (Fe-deprived) and 5 μM Fe_3–EDTA (Fe-deficient) respectively. The volume of nutrient solution was adjusted to the same volume by MilliQ water daily, the nutrient solution changed every third day. Plant leaves were sampled after 20 days of differential iron supply for various analyses except for those stated otherwise.

2.3. Iron localisation and concentration

Iron content was analysed in the acidic (HNO_3:$HClO_4$, 3:1) leaf tissue digest prepared in MilliQ water (10 mg dry weight/ml). The samples were incubated for 24 h at 37 °C in the presence of 5 mM 2,2′ bipyridine and 100 mM ascorbic acid (pH 7.0) prepared in MilliQ water. For each sample both a reactive blank, and a sample blank without adding 2,2′-bipyridine were prepared and absorbance was measured at 520 nm (Gonzalez and Puntarulo, 2011). A standard curve in a concentration range from 0 to 100 μM iron was used.

Iron was localized in the leaves with Perls/DAB technique (Roschzttardtz et al., 2010). The leaves were vacuum infiltrated with equal volumes of 4% HCl (v/v) and 4% K-ferrocyanide (w/v) for 15 min and incubated for 30 min at room temperature. After washing with distilled water, the leaves were incubated in a methanolic solution containing 0.01 M NaN_3 and 0.3% H_2O_2 (v/v) for 1 h, and then washed with 0.1 M phosphate buffer (pH 7.4). For the intensification reaction the leaves were incubated for 10–30 min in a 0.1 M phosphate buffer (pH 7.4) solution containing 0.025% DAB (w/v), 0.005% H_2O_2 (v/v), and 0.005% $CoCl_2$ (w/v) (intensification solution). The reaction was stopped by rinsing with distilled water. Pigments were removed with methanol and mounted on slides with glycerol and observed under the microscope.

2.4. Chlorophylls and carotenoids

Chlorophylls and carotenoids were determined in 80% (v/v) acetone extract of the young fully expanded leaf (Lichtenthaler, 1987). The colour intensity of the filtered extract was measured at 663, 646 and 470 nm for chlorophyll *a*, chlorophyll *b* and total carotenoids respectively.

2.5. Chlorophyll fluorescence

Chlorophyll fluorescence was measured using a pulse-amplitude-modulated fluorescence monitoring system, portable PAM-2000 (Walz GmbH, Effeltrich, Germany). The effective quantum yield of PSII [Y(II)] and effective electron transport rate (ETR) was measured following procedures of the manufacturer (Anonymous, 2005). Numerical values of chlorophyll fluorescence parameters were evaluated by using the supplied software ImagingWin 2.

2.6. Superoxide anion radical

Leaves were vacuum infiltrated with a 0.1 mg ml^{-1} solution of *p*-nitroblue tetrazolium (NBT) in 0.25 M HEPES buffer (pH 7.6) for 15 min and then incubated at 25 °C in the dark for 2 h. Controls or blanks in presence of $MnCl_2$ (scavengers of $O_2^{\bullet -}$) were also performed simultaneously by adding 10 mM of $MnCl_2$ to the buffer (Tewari et al., 2006). Pigments present in the leaf were cleared in

80% ethanol (v/v) for 20 min at 70 °C and then mounted in a lactic acid, phenol and water mixture (1:1:1, v/v). The mounted leaf was photographed under stereo microscope. Superoxide was quantified in terms of formazan formation in the third expanded leaf of a shoot. Formazan was extracted by pyridine from the leaf tissue and quantified by absorbance at 510 nm Concentration calculation was performed using an extinction coefficient of 11,000 M^{-1} cm^{-1} (Suh et al., 1999).

2.7. Hydrogen peroxide

Hydrogen peroxide was measured by monitoring the fluorescence of dichlorofluorescein (DCF), which is the oxidation product of H_2DCF-DA (Gerber and Dubery, 2003). Protoplasts were isolated from young expanded leaves of different iron treatments as described previously (Watanabe et al., 2002). The protoplasts were washed and re-suspended in 0.6 M sorbitol in 5 mM MES buffer (pH 5.8) and 5 mM $CaCl_2$, and loaded with 100 μM H_2DCF-DA for 30 min in darkness. Fluorescence intensity was monitored at an excitation wavelength of 485 nm and emission wavelength of 538 nm. In addition, 0.06 mm-thick sections of leaves that were loaded with 100 μM H_2DCF-DA for 30 min at 25 °C under the same conditions as mentioned above and observed with confocal laser microscopy (Leica TCS-SP2). H_2O_2 formation (green fluorescence) shows in blue when merged with the red channel.

2.8. Lipid peroxidation

Lipid peroxidation was determined in terms of TBA reactive substance (TBARS) that was calculated from the difference in absorbance at 532 and 600 nm using an extinction coefficient of 155 mM^{-1} cm^{-1} (Heath and Packer, 1968).

2.9. Ascorbate concentration

Fresh leaf tissue (250 mg) was homogenized in 2.0 ml of 10% (w/v) TCA and centrifuged for 5 min at 10,000 × *g* total ascorbate (after reducing DHA to AA by DTT), and AA in the supernatant, were measured as Fe^{2+}–bipyridine complex (absorbance maximum at 525 nm) that was formed after reduction of Fe^{3+} (supplied as $FeCl_3$) by AA (Law et al., 1983). DHA content was calculated from the difference between total ascorbate and AA.

2.10. Enzyme activities

Leaf tissue (0.5 g) was frozen with liquid N_2 and homogenized in 2.0 ml chilled 50 mM potassium phosphate buffer (pH 7.0) containing 0.5% (w/v) insoluble polyvinylpolypyrrolidone and 1.0 mM phenylmethylsulfonylfluoride. The homogenate was filtered through two-fold Miracloth™ (Merck Chemicals Ltd., Nottingham, UK) and centrifuged at 20,000 × *g* for 10 min at 2 °C. The supernatant was stored at 2 °C and used for enzyme assays within 4 h.

NADPH oxidase-like (NOX-like) enzyme activity was determined as described previous with minor modifications (Tewari et al., 2012). This modified assay is based on the reduction of NBT by superoxide anion radical generated by the oxidation of NADPH. The reaction mixture contained 10 μl of enzyme extract, 0.1 mM NBT, 0.2 mM NADPH, 0.1 mM $MgCl_2$, and 1.0 mM $CaCl_2$ in 1 ml of 50 mM Tris–HCl (pH 7.4). The reaction was initiated by the addition of NADPH, and the change in absorbance at 530 nm was recorded. Rates of reduction of NBT were calculated using an extinction coefficient of 12.8 mM^{-1} cm^{-1}. NADPH oxidase-like activity was presented as μmol NBT reduced min^{-1} mg^{-1} protein.

Superoxide dismutase (SOD) activity was assayed by measuring its ability to inhibit the photochemical reduction of NBT at 560 nm The reaction mixture (5.0 ml) contained 25 mM phosphate buffer (pH 7.8), 65 μM NBT, 2 μM riboflavin, enzyme extract, and 15 μl N,N,N,N-tetramethylethylenediamine (Tewari et al., 2006). The reaction mixture was exposed to light (350 μmol m^{-2} s^{-1}) for 15 min. The amount of SOD corresponding to 50% inhibition of the reaction was defined as one unit of enzyme.

Catalase (CAT) activity was measured in a reaction mixture containing 10 μl of the extract, 3 ml of 5 mM H_2O_2 in 50 mM potassium phosphate (pH 7.0). The decrease in absorbance at 240 nm was monitored for 3 min, and rate of decrease H_2O_2 was calculated using an extinction coefficient of H_2O_2 at 240 nm of 0.0435 mM^{-1} cm^{-1} (Tewari et al., 2012). CAT activity was presented as μmol H_2O_2 decomposed min^{-1} (unit) mg^{-1} protein.

Peroxidase (POD) activity was estimated in a reaction mixture containing 5 ml 100 mM phosphate buffer (pH 6.5), 1.0 ml 0.1% DAB (v/v), 1.0 ml 0.01% H_2O_2 (v/v), and leaf extract (10 μl) and change in absorbance was measured at 485 nm (Tewari et al., 2005). Enzyme activity is expressed as ΔAbs 0.01 min^{-1} (unit) mg^{-1} protein basis.

Alkaline protease activity was assayed by using a azocasein digestion assay (Casano et al., 1989). Reaction mixture contained 0.1 ml of crude extract, 0.3 ml of 0.5% azocasein and 0.6 ml of 50 mM Tris–HCl buffer (for pH 8.4). The mixture was incubated for 2 h at 37 °C and the reaction was stopped by adding 2 ml of ice-cold 12% trichloroacetic acid (TCA). Precipitated proteins were removed by centrifugation (10,000 × *g*, 10 min), and absorbance of supernatant was measured at 340 nm. One unit of azocaseinolytic activity was defined as increase of 0.01/min at 340 nm.

Deoxyribonuclease (DNAse) activity was assayed by measuring the release of acid-soluble material from denatured calf thymus DNA (Blank and McKeon, 1989). Assay mixtures (300 μl) containing 0.1% DNA, 0.1% bovine serum albumin, 0.1 M Tris–HCl (pH 7.5), and leaf extract (10 μl) were incubated for 60 min at 37 °C. After addition of 1 ml 3.4% perchloric acid (v/v), suspensions were held on ice for 10 min and then centrifuged for 5 min at 14,000 × *g*. Absorbance of the supernatants was read at 260 nm, and the difference between blank and sample was determined. The given unit is that amount of enzyme that yields an absorbance change of 1 min^{-1} ml^{-1} incubation mixture.

2.11. Cell death assay

Leaves were harvested and stained with lactophenol–trypan blue (10 ml lactic acid, 10 ml glycerol, 10 g phenol, 10 mg trypan blue, dissolved in 10 ml distilled water) to visualize dead cells (Koch and Slusarenko, 1990). Leaves were boiled for approximately 1 min in the stain solution and then decolourized by lactophenol (10 ml lactic acid, 10 ml glycerol, 10 g phenol) and ethanol (ratio 1:2) for several hours to remove pigments. Images were taken with a digital camera.

2.12. Nuclear morphology

Protoplasts were isolated and fixed in 2% glutaraldehyde in sorbitol buffer (10 mM phosphate buffer, 0.6 M sorbitol, pH 7.4) for 2 h at room temperature and stained with DAPI (Watanabe et al., 2002). The protoplasts were washed and re-suspended in the sorbitol buffer. DAPI was added to the suspension at the final concentration 10 μg ml^{-1} and visualisation was performed using a fluorescence microscope (Olympus BX41, Olympus Austria GmbH, Vienna) with an excitation filter of 340 nm and a barrier filter of 400 nm

2.13. DNA fragmentation

Leaf tissue nuclear DNA was extracted according to the manufacturer's protocol for plant DNA isolation reagent (Takara Biotechnology (Dalian) Co. Ltd., Takara Bio Inc.). Nuclear DNA was loaded and run on a 2% (w/v) agarose gel at constant 100 V. DNA was visualized by staining with 0.1 μg ml^{-1} ethidium bromide.

2.14. Protein concentration and caspase 3, activity assays

Leaf tissue was ground in liquid N_2. The powder was lysed in caspase lysis buffer (50 mM HEPES (pH 7.4), 5 mM CHAPS, 5 mM DTT) at 4 °C for 30 min. Lysates were centrifuged at 28,000 × *g* for 30 min and protein concentration was determined in the supernatant (Bradford, 1976).

Caspase-3-like activity was measured in leaf extract using a fluorometric caspase 3 assay kit (Sigma) as per suppliers' protocol. An appropriate volume of extract (5 μl) was mixed with 200 μl of caspase reaction mixture (20 mM HEPES (pH 7.4), 2 mM EDTA, 5 mM DTT, 0.1% CHAPS and 16.66 μM Ac–DEVD–AMC) with or without 2 μM of DEVD–CHO (caspase 3 inhibitor). Samples were incubated at 30 °C for 2 h and the fluorescence was measured using a fluorescent spectrophotometer at an excitation/emission wavelength of 380/445 nm. Enzyme units were calculated using a 7-amino-4-methylcoumarin (AMC) standard curve.

2.15. SDS-PAGE and in gel assay of DNAse activity

DNAse was detected by activity staining in 12.5% SDS-PAGE (Blank and McKeon, 1989). Gels were loaded with leaf extracts heated for 2 min at 100 °C in buffer containing 2% SDS and 10 mM dithiothreitol. Separation gels contained 0.3 mg of denatured calf thymus DNA in the matrix and were run at room temperature. After electrophoresis, enzymes were renatured by gentle agitation of the gels for 2 h in 125 ml 0.01 M Tris–HCl (pH 7.5) with three changes of solution at 50 °C. Thereafter, gels were incubated at room temperature in 0.1 M Tris–HCl (pH 7.5) for 15 h to allow enzymatic degradation of embedded DNA and then stained with toluidine blue.

2.16. Statistics

Significant differences between means were determined by ANOVA and subsequent multiple pairwise comparison by 95% Fischer's LSD using Sigma Plot 11 (Systat Software Inc., San Jose, CA). Principal component analysis was performed to determine variable correlation with treatments using Primer 6 (Primer E Ltd., Plymouth, UK). Pearson's correlation coefficients with the separate principle component axes were calculated for all variables.

3. Results

3.1. Iron concentration

Leaf tissue iron concentration was related to the supplied amounts and decreased in the leaf tissue receiving no iron (iron-deprived) or low iron (iron-deficient) supply (Fig. 1A). In situ localisation of iron in the leaf tissue identified stomata guard cells as major accumulation site. Iron-deprived and -deficient leaves showed very faint brown colouration; sufficiently supplied leaves were characterized by intensely coloured stomata guard cells (Fig. 1B).

3.2. Reduced iron supply decreased chloroplastic pigments, cell size and plant growth

Iron deficiency and deprivation decreased amounts of chloroplastic pigments, chl *a*, chl *b* and carotenoids (Fig. S1A). The ratio of chl *a*/*b*, however, was not affected. The carotenoids/chlorophyll ratio was enhanced especially in iron-deprived plants (Fig. S1B). These plants also showed retarded growth with reduced cell size, which was reflected by decreased shoot and total biomass (Fig. S2A) Shoot to root ratio, however, remained unaffected (Fig. S2B).

3.3. Iron deprivation suppressed photosynthesis efficiency

Iron deprivation and deficiency affect photosynthesis, effective quantum yield [Y(II)] and effective electron transport rate (ETR). The effect was more severe in the plants receiving no iron; Y(II) decreased to the lowest level even at the lowest light intensity (Fig. 2A and B). These decreases in Y(II) and effective ETR reflect damages of PS II and electron transport chains in iron-deprived plants.

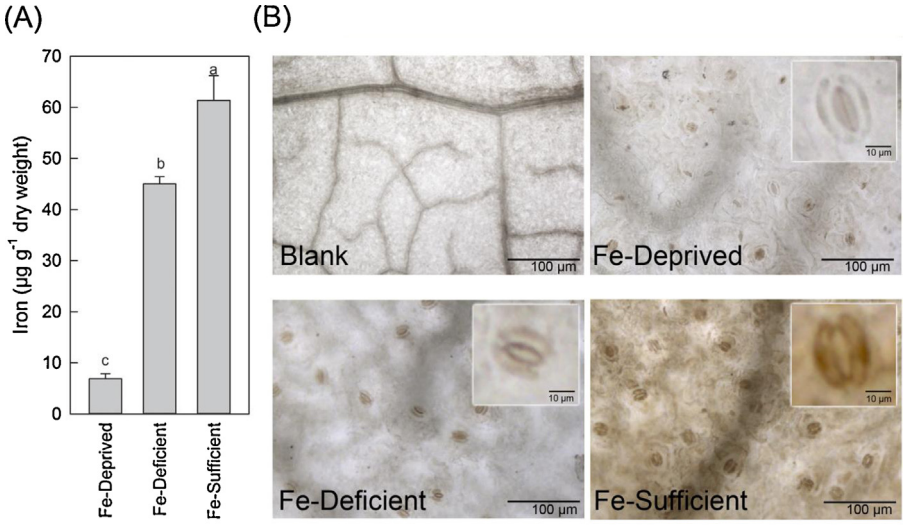

Fig. 1. Iron status in young *Brassica napus* leaves of Fe-deprived (0 μM Fe), Fe-deficient (5 μM Fe) and Fe-sufficient (50 μM Fe) plants: (A) iron concentration as determined by bipyridine extraction; (B) in situ localisation by Perl reagent. Vertical bars: mean ± SE (n = 6). Bars carrying different letters are significantly (95% Fisher LSD).

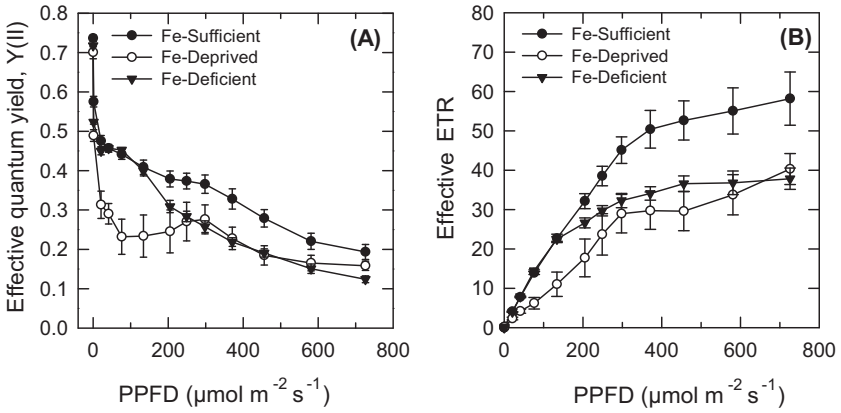

Fig. 2. Photosynthetic activity in young *Brassica napus* leaves of Fe-deprived (0 μM Fe), Fe-deficient (5 μM Fe) and Fe-sufficient (50 μM Fe) plants: (A) effective PS II quantum yield Y (II); (B) relative apparent electron transport rate (ETR). Each data point represents mean ± SE ($n = 6$).

3.4. Iron deprivation caused ROS accumulation

Iron-deprivation caused about seven-fold higher accumulation of $O_2^{\bullet-}$ compared to the leaf tissues of iron-deficient or iron-sufficient plant. Accumulation of $O_2^{\bullet-}$ was quite intense along the vascular tissue (veins) but it also accumulated in other tissue regions of iron-deprived leaves (Fig. 3A). No cell shrinking occurred. Plants receiving deficient and sufficient supply of iron

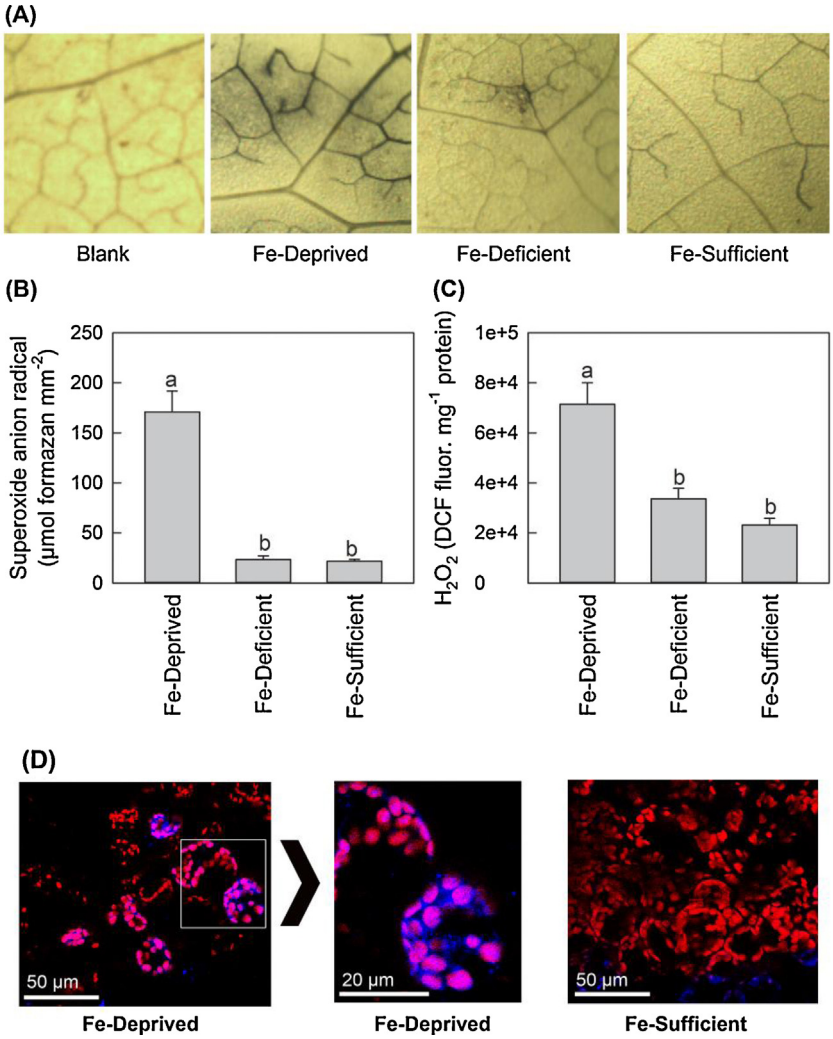

Fig. 3. Relative superoxide anion radical and hydrogen peroxide levels in young *Brassica napus* leaves of Fe-deprived (0 μM Fe), Fe-deficient (5 μM Fe) and Fe-sufficient (50 μM Fe) plants: (A) in situ $O_2^{\bullet-}$ accumulation (purple blue formazan); (B) relative formazan ($O_2^{\bullet-}$) quantities; (C) H_2O_2 (relative DCF fluorescence); (D) hydrogen peroxide (DCF fluorescence shown as blue colour when merged with red chlorophyll fluorescence) in the chloroplasts of Fe-deprived and Fe-sufficient leaves transverse sections. Vertical bars: mean ± SE ($n = 6$). Bars carrying different letters are significantly different (95% Fisher LSD).

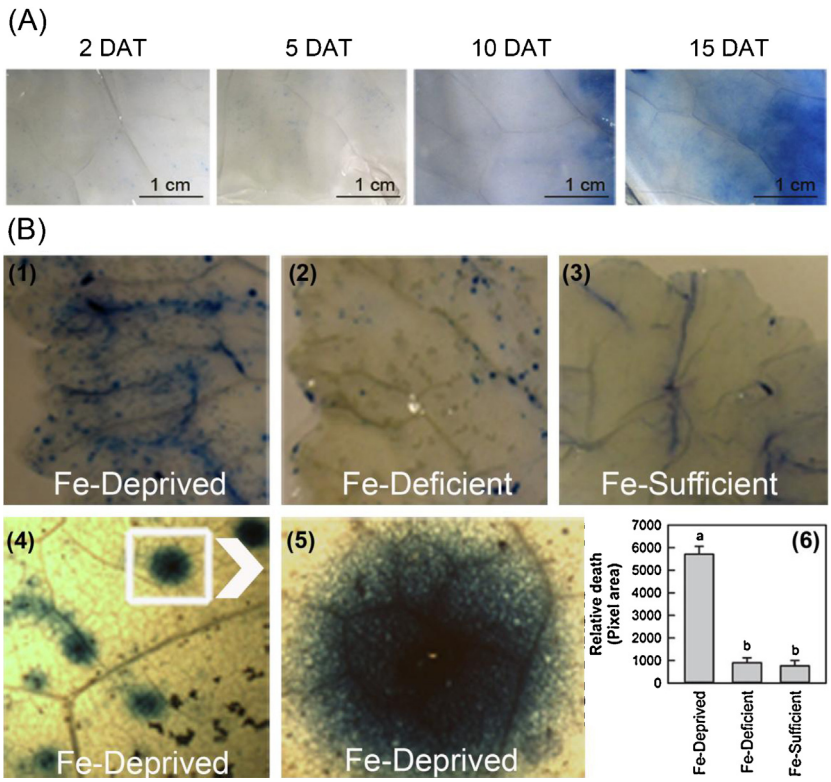

Fig. 4. Cell death development in young *Brassica napus* leaves of Fe-deprived (0 μM Fe), Fe-deficient (5 μM Fe) and Fe-sufficient (50 μM Fe) plants: (A) cell death development at 2, 5, 10 and 15 days (DAT) at 0 μM Fe; (B) cell death (1–3) at differential iron supply levels after 20 DAT, (4) microscopic image, (5) magnified view of a lesion, (6) relative cell death quantitation. Vertical bars: mean ± SE ($n = 6$). Bars carrying different letters are significantly different (95% Fisher LSD).

showed very similar and lower accumulation of $O_2^{\bullet -}$ in the leaves (Fig. 3A and B). Moreover, iron-deprived plants also showed higher levels of H_2O_2 as suggested by intense DCF fluorescence in the leaf tissue protoplasts (Fig. 3C). Moreover, confocal laser microscopy provided evidence that chloroplasts represented the major H_2O_2 source in iron-deprived leaves (Fig. 3D).

3.5. Iron deprivation induced cell death in the chlorotic leaves

Trypan blue treatment pointed to cell death processes occurring in the chlorotic tissues of iron-deprived plants (Fig. 4). The first symptoms were observed in leaves 10 days after iron deprivation treatment had started. Cell death progressed further with on-going iron deprivation (Fig. 4A). Leaves of iron-deficient and -sufficient plants, which showed no chlorosis, did not show comparably intensely stained tissue areas to those of iron-deprived leaves (Fig. 4B).

3.6. Iron deprivation caused chromatin condensation and DNA fragmentation

Nuclear condensation was observed in the leaf protoplasts of iron-deprived plants. While iron-deprived leaf protoplasts showed highly condensed and small circular nuclei, the protoplasts of plants receiving deficient or sufficient iron supply were larger in size with relatively big nuclei that displayed condensed (heterochromatin) and non-condensed (euchromatin) regions inside the nucleus (Fig. 5A). Some of the nuclei of these plant cells were semi-circular or elliptical in shape (Fig. 5A). Iron deprivation induced a single isoform of DNAse (Fig. 5B) and also induced DNA fragmentation, which is indicated by low molecular weight bands or smear separated on the agarose gel (Fig. 5C). Plants that received deficient or sufficient iron supply did not show DNA fragmentation (Fig. 5C). Iron deficient and iron sufficient leaves also did not show any *in gel* DNAse activity band (Fig. 5B).

3.7. Reduced iron supply effects on enzyme activities

NADPH oxidase-like activity was not affected significantly by variable iron supply in *B. napus* plants (Fig. 6A), but SOD and POD activities were enhanced in iron-deprived and iron-deficient leaves (Fig. 6B and C). CAT activity was decreased in iron-deprived and -deficient leaves (Fig. 6D). Iron deprivation activated caspase-3-like, alkaline protease and DNAse activites in *B. napus* leaves (Fig. 6E and F). Iron deficiency also activated caspase-3-like activity but its increase was relatively moderate compared to iron-deprived plants (Fig. 6A). No significant changes were observed in alkaline protease and DNAse activities of iron-deficient when compared to those of iron-sufficient plants (Fig. 6E and F).

3.8. Iron deprivation enhanced AA and DHA concentration but decreased lipid peroxidation

Iron deprivation enhanced both AA and DHA concentration in the leaf, iron deficiency enhanced AA but not DHA levels. Compared to iron-deficient leaves, the DHA/AA ratio was larger both in iron-deprived and -sufficient plants (Fig. 7A and B). Iron-deprived and -deficient leaves showed lower lipid peroxidation compared to iron-sufficient. Leaf TBARS levels correlated with levels of iron supply and were highest in iron-sufficient plants (Fig. 7C).

3.9. Principle component analysis

The first principle component axis separated the iron-deprived from the iron-deficient and iron-sufficient plants, representing 79.9% of the total sample variation (Fig. 8). Iron leaf content

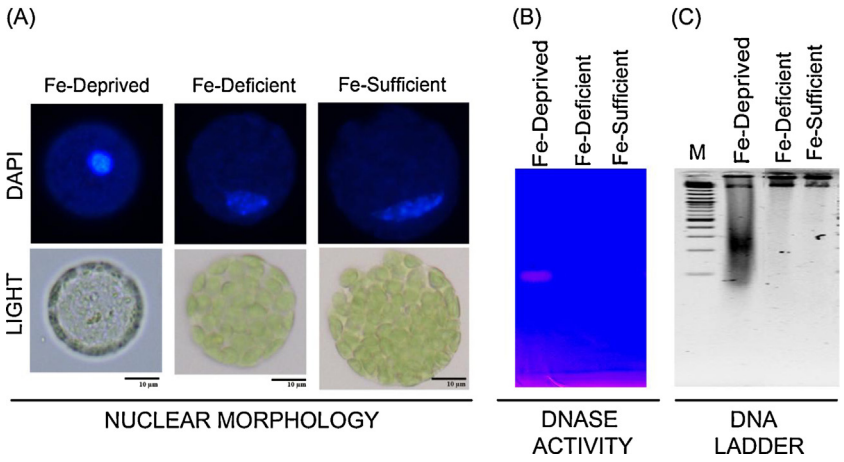

Fig. 5. Cell death processes in young *Brassica napus* leaves of Fe-deprived (0 μM Fe), Fe-deficient (5 μM Fe) and Fe-sufficient (50 μM Fe) plants: (A) chromatin condensation (DAPI) and nuclear morphology (light microscopy) in protoplasts; (B) DNAse activity on SDS-polyacrylamide gel; (C) DNA laddering assay on agarose gel.

($r = 0.96$), chlorophyll content ($r = 0.91$), CAT activity ($r = 0.92$) and TBARS levels ($r = 0.81$) showed positive correlations; Cell death ($r = -0.95$), caspase-3 activity ($r = -0.96$), $O_2^{\bullet -}$ levels ($r = -0.94$), H_2O_2 levels ($r = -0.91$), SOD activity ($r = -0.82$), protease activity ($r = -0.81$), AA ($r = -0.74$), DHA ($r = -0.87$) and DNAse activity ($r = -0.66$), correlated negatively with PC1.

4. Discussion

Here we provide evidence that ROS accumulation especially correlates with non-autolytic PCD processes in iron-deprived but to a lesser extent in iron-deficient *B. napus* leaves. ROS activity was detected by one electron oxidation of $O_2^{\bullet -}$ and H_2O_2

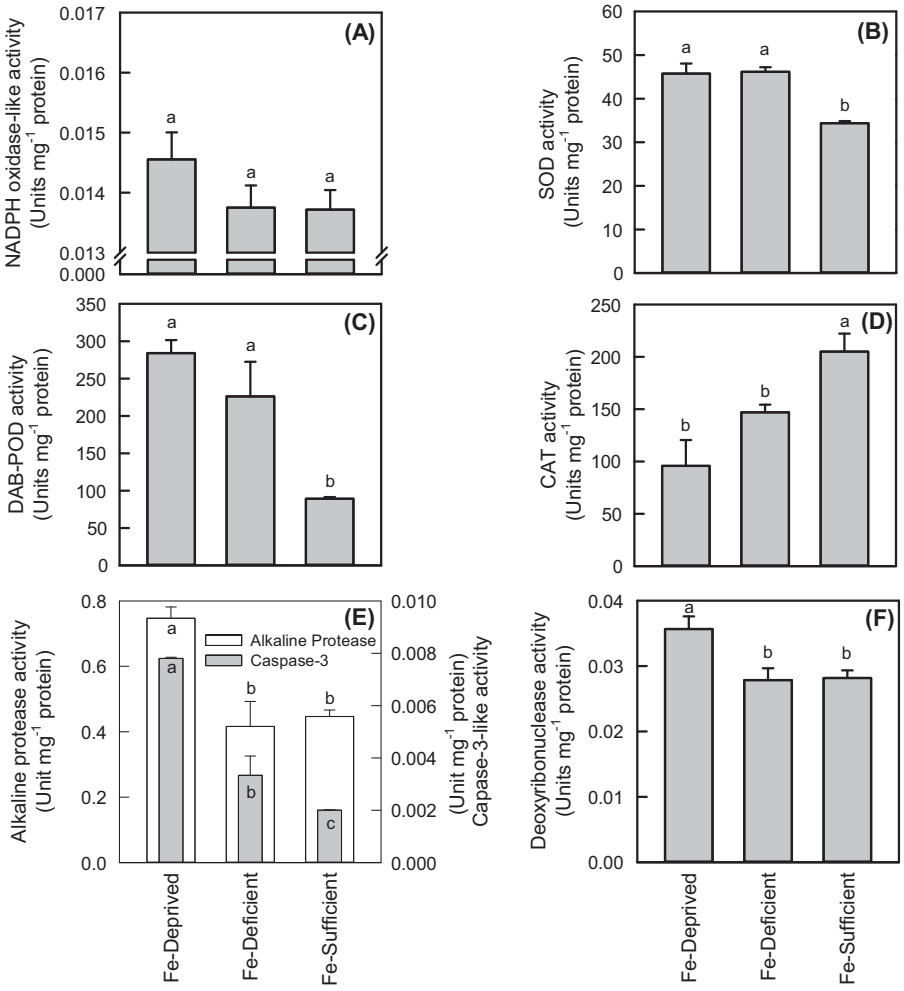

Fig. 6. Enzymes activities in young *Brassica napus* leaves of Fe-deprived (0 μM Fe), Fe-deficient (5 μM Fe) and Fe-sufficient (50 μM Fe) plants: (A) NADPH oxidase-like; (B) SOD; (C) DAB peroxidase (POD); (D) CAT; (E) alkaline protease (white bars) and caspase-3 (grey bars); (F) deoxyribonuclease (DNAse). Vertical bars: mean ± SE ($n = 6$). Bars carrying different letters are significantly different (95% Fisher LSD).

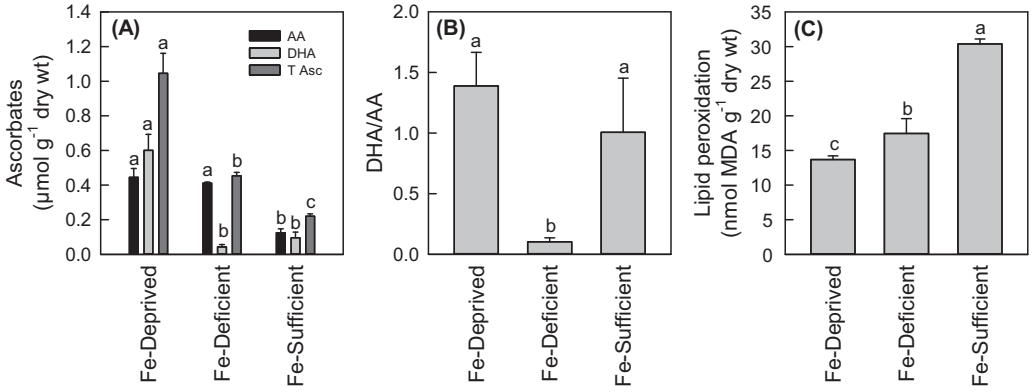

Fig. 7. Ascorbic acid and lipid peroxidation in young *Brassica napus* leaves of Fe-deprived (0 μM Fe), Fe-deficient (5 μM Fe) and Fe-sufficient (50 μM Fe) plants: (A) ascorbic acid (AA), dehydroascorbic acid (DHA) and total ascorbate (T Asc); (B) DHA/AA ratio; (C) lipid peroxidation. Vertical bars: mean ± SE ($n = 6$). Bars carrying different letters are significantly different (95% Fisher LSD) and apply to AA, DHA and T Asc concentrations in each treatment respectively.

by two electron reduction reactions. Lower TBARS values suggest that •OH formation occurred to a lesser extent. Iron deprivation affects the biosynthesis of chloroplastic pigments negatively (Kumar et al., 2010; Tewari et al., 2005). Chlorosis usually is accompanied by decreased CAT activity (Brown and Hendricks, 1952). Accordingly, iron-deprived leaves also showed lower CAT activity. This represents a specific iron effect because other factors triggering non-autolytic PCD, such as temperature or pathogen stress, increase CAT and POD activities (Locato et al., 2008). Iron-deprivation, however, affected peroxisome-located catalase more than the cytosolic DAB-POD activity. Both rely on iron as co-factor (Broadley et al., 2012) and can be restored by iron-EDTA sprays (Agarwala and Mehrotra, 1977). Acting in concert, this may explain why H_2O_2 amounts increased and •OH decreased in iron-deprived leaves.

Reportedly, iron deficiency impairs photosynthesis (Molassiotis et al., 2006; Saito et al., 2010). Accordingly, effective quantum yield Y(II) and effective electron transport rate ETR in iron-deficient and -deprived were lower than in -sufficient plants. Iron is an essential constituent of several proteins of the chloroplast's electron transport chain (Imsande, 1998). Hindered electron transport rates in iron-deprived leaf chloroplasts results in one-electron transfers to molecular oxygen, generating excessive levels of $O_2^{\bullet-}$ (Foyer et al., 2012). We can show that $O_2^{\bullet-}$ arises in chloroplasts with H_2O_2 accumulating in the chloroplasts (Fig. 3D). $O_2^{\bullet-}$ accumulation has already been reported for iron-deficient maize (Tewari et al., 2005). The fact that NADPH oxidase-like activity was not affected by iron-deficiency additionally correlates with the observation that chloroplasts represent the major ROS source. In concordance, $O_2^{\bullet-}$ production is met by increased SOD activity in iron-deprived rapeseed leaves. Increased SOD activity leads to H_2O_2 accumulation (Halliwell, 2006). Despite higher levels of $O_2^{\bullet-}$ and H_2O_2 in iron-deprived and -deficient than in -sufficient plants, TBARS levels were lower. Possibly, lipid peroxidation in iron-deprived plants becomes retarded due to low availability of catalytic (functional) iron, which highly efficiently catalyses the OH• producing Fenton reaction (Broadley et al., 2012; Halliwell, 2006). Unavailability of catalytically active iron might be due to increased ferritin expression, a recognized iron storage protein, in iron-deficient plants (Graziano and Lamattina, 2007). Similarly as in case of CAT, iron deficiency can affect lipoxygenase activity negatively, another iron-dependent enzyme (Boyer and Vanderploeg, 1986). Lower TBARS levels in iron-deficient pea and maize plants also have been attributed to functional iron deficit (Iturbe-Ormaetxe et al., 1995; Tewari et al., 2005). Summing up, the obtained results suggest that the oxidative stress in iron-deprived rapeseed leaf tissues was caused more by $O_2^{\bullet-}$ than OH• formation. As an antioxidant defence, AA can reduce H_2O_2 to H_2O by a two-electron transfer and, conversely, is oxidized to DHA (Davey et al., 2000). In iron-deprived plants, especially the amounts of DHA increased, suggesting that more AA was oxidized to DHA as a consequence of H_2O_2 reduction. In the iron-deprived rapeseed plants, the incapacity of the antioxidant defence system to quench H_2O_2 levels suggests that H_2O_2 acts as trigger for non-autolytic PCD in this specific situation (Fig. 9). A possible explanation for the breakdown of the DHA/AA ratio in iron-deficient plants (Fig. 7B) could be that concomitant stimulation of the Asada–Foyer–Halliwell pathway, which contributes to the AA regeneration (Asada, 1999) efficiently reduces DHA amounts. In a more complex reality, however, besides the AA/DHA ratios and concentrations, which were determined in this study, the contributions of other antioxidant low-molecular-weight compounds, such as flavonoids and various antioxidant enzymes have to be considered too (Foyer and Noctor, 2005; Slesak et al., 2007).

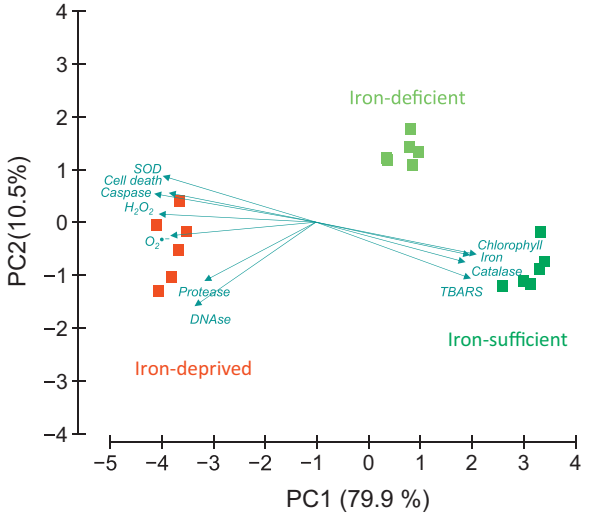

Fig. 8. Principle component analysis of analysed factors that characterize variable iron supply in young *Brasssica napus* leaves of Fe-deprived (0 μM Fe), Fe-deficient (5 μM Fe) and Fe-sufficient (50 μM Fe) *Brassica napus* plants ($n = 6$).

Excessive electrolyte leakage from iron-deficient *Arabidopsis* leaves also suggests membrane damage and PCD in iron-deficient leaves (Msilini et al., 2009). Numerous studies exist that document the efficacy of low-dose H_2O_2 to induce PCD in plant protoplasts (Maccarrone et al., 2000) and cell lines (Ge et al., 2005; Houot et al., 2001; Sun et al., 2012). Evidence that non-autolytic PCD actually occurred in iron-deprived rapeseed leaf tissues was provided

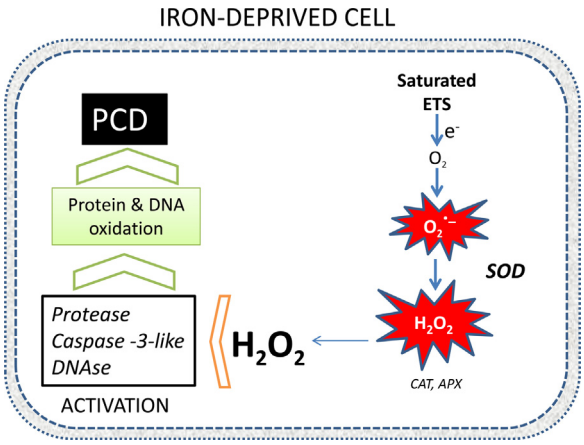

Fig. 9. Schematic model of ROS signalling in programmed cell death in Fe-deprived chlorotic leaves of *Brassica napus* plants. Leakage of electron from chloroplastic ETS form $O_2^{\bullet-}$, which directly or via H_2O_2 activated caspase 3-like, protease and DNAse activities lead to protein and DNA lyses causing non-autolytic PCD.

by the following results: elevated DNAse, alkaline protease and caspase-3-like activities result in DNA and protein lyses (Kempe et al., 2006; Koc et al., 2006; Kuthanova et al., 2008; Piszczek and Gutman, 2007; Reape et al., 2008). Although no genomic evidence is yet available for existence of caspase genes in plants, however, plants undergoing PCD do show caspase-3-like activity (Belenghi et al., 2004; Chichkova et al., 2010, 2012; Coffeen and Wolpert, 2004; Ge et al., 2005; Sun et al., 2012). DNA fragmentation (Jiang et al., 2008) and chromatin condensation (Simeonova et al., 2000) provided additional evidence for the onset of PCD in the iron-deprived leaves of *B. napus* plants, which was non-autolytic due to the absence of cell shrinking (van Doorn, 2011).

We also noted certain necrotic lesions in iron-deprived chlorotic leaves at an advanced stage of iron deprivation. The fact that iron-sufficient leaves accumulate considerable amounts in stomata guard cells implies that stomata function also may be affected by iron deficiency. Disturbed water relations might represent an additional stress for the affected plant. These assumption are supported by a study that detected transient stomata opening in iron-deficient chlorotic pear and peach leaves after abscission; this phenomenon is known as Iwanoff effect (Fernandez et al., 2008). Leakage of electrons from electron transport chains in chloroplasts (reduced PSII and electron transport efficacy) and probably also mitochondria represents the major source of ROS in iron-deprived plants. Therefore, non-autolytic PCD has to be expected occurring in these plants under conditions of severe and prolonged iron-deficiency. Activation of protease, DNase and caspase-3-like activity, which is regarded as a hallmark of PCD, was observed in iron-deficient plants exclusively. A multivariate analysis of the various factors that were assessed in this study underpins our conclusions that are summarized in Fig. 9. In as much this signalling event occurs generally in plants and how variable it is, however, has to be explored by further studies.

Acknowledgements

RK Tewari's research was supported by a Lise Meitner fellowship (M1303-B20) of the Austrian Science Fund (FWF). The authors are also grateful to the Departments of Cell Imaging and Ultrastructure Research (CIUS) and Molecular System Biology (MOSYS), University of Vienna, for access to microscopy and gel electrophoresis facilities respectively. We also thank Barbara S. Sixt (Department of Microbial Ecology) for support with caspase-3 assay and Dr. Gert Bachmann (MOSYS) for statistical advice. Thoughtful comments from two anonymous reviewers helped to improve the manuscript considerably.

Appendix A. Supplementary data

Supplementary data associated with this article can be found, in the online version, at http://dx.doi.org/10.1016/j.envexpbot.2013.03.006.

References

Abdelmajid, K., Karim, B.H., Chedly, A., 2008. Symbiotic response of common bean (*Phaseolus vulgaris* L.) to iron deficiency. Acta Physiologiae Plantarum 30, 27–34.
Agarwala, S.C., Mehrotra, N.K., 1977. Catalase and peroxidase in leaves of iron-deficient plants. Proceedings of the Indian Academy of Sciences Section B 86, 55–60.
Anonymous, 2005. MAXI-IMAGING-PAM. Heinz Walz GmbH, Effeltrich.
Asada, K., 1999. The water–water cycle in chloroplasts: scavenging of active oxygens and dissipation of excess photons. Annual Review of Plant Physiology and Plant Molecular Biology 50, 601–639.
Belenghi, B., Salomon, M., Levine, A., 2004. Caspase-like activity in the seedlings of *Pisum sativum* eliminates weaker shoots during early vegetative development by induction of cell death. Journal of Experimental Botany 55, 889–897.
Blank, A., McKeon, T.A., 1989. Single-strand-preferring nuclease activity in wheat leaves is increased in senescence and is negatively photoregulated. Proceedings of the National Academy of Sciences of the United States of America 86, 3169–3173.
Boyer, R.F., Vanderploeg, J.R., 1986. Iron metabolism in higher plants – the influence of nutrient iron on bean leaf lipoxygenase. Journal of Plant Nutrition 9, 1585–1600.
Bradford, M.M., 1976. Rapid and sensitive method for quantitation of microgram quantities of protein utilizing principle of proteindye binding. Analytical Biochemistry 72, 248–254.
Broadley, M., Brown, P.I.C., Rengel, Z., Zhao, F., 2012. Function of nutrients: micronutrients. In: Marschner, P. (Ed.), Marschner's Mineral Nutrition of Higher Plants. Elsevier, Amsterdam.
Brown, J.C., Hendricks, S.B., 1952. Enzymatic activities as indications of copper and iron deficiencies in plants. Plant Physiology 27, 651–660.
Casano, L.M., Desimone, M., Trippi, V.S., 1989. Proteolytic activity at alkaline pH in oat leaves: isolation of an aminopeptidase. Plant Physiology 91, 1414–1418.
Chichkova, N.V., Shaw, J., Galiullina, R.A., Drury, G.E., Tuzhikov, A.I., Kim, S.H., Kalkum, M., Hong, T.B., Gorshkova, E.N., Torrance, L., Vartapetian, A.B., Taliansky, M., 2010. Phytaspase, a relocalisable cell death promoting plant protease with caspase specificity. EMBO Journal 29, 1149–1161.
Chichkova, N.V., Tuzhikov, A.I., Taliansky, M., Vartapetian, A.B., 2012. Plant phytaspases and animal caspases: structurally unrelated death proteases with a common role and specificity. Physiologia Plantarum 145, 77–84.
Coffeen, W.C., Wolpert, T.J., 2004. Purification and characterization of serine proteases that exhibit caspase-like activity and are associated with programmed cell death in *Avena sativa*. Plant Cell 16, 857–873.
Connolly, E.L., Guerinot, M., 2002. Iron stress in plants. Genome Biology 3, REVIEWS1024.
Davey, M.W., Van Montagu, M., Inze, D., Sanmartin, M., Kanellis, A., Smirnoff, N., Benzie, I.J.J., Strain, J.J., Favell, D., Fletcher, J., 2000. Plant L-ascorbic acid: chemistry, function, metabolism, bioavailability and effects of processing. Journal of the Science of Food and Agriculture 80, 825–860.
Donnini, S., Dell'Orto, M., Zocchi, G., 2011. Oxidative stress responses and root lignification induced by Fe deficiency conditions in pear and quince genotypes. Tree Physiology 31, 102–113.
Fernandez, V., Eichert, T., Del Rio, V., Lopez-Casado, G., Heredia-Guerrero, J.A., Abadia, A., Heredia, A., Abadia, J., 2008. Leaf structural changes associated with iron deficiency chlorosis in field-grown pear and peach: physiological implications. Plant and Soil 311, 161–172.
Foyer, C.H., Neukermans, J., Queval, G., Noctor, G., Harbinson, J., 2012. Photosynthetic control of electron transport and the regulation of gene expression. Journal of Experimental Botany 63, 1637–1661.
Foyer, C.H., Noctor, G., 2005. Redox homeostasis and antioxidant signaling: a metabolic interface between stress perception and physiological responses. Plant Cell 17, 1866–1875.
Frey, P.A., Reed, G.H., 2012. The ubiquity of iron. ACS Chemical Biology 7, 1477–1481.
Ge, Z.Q., Yang, S., Cheng, J.S., Yuan, Y.J., 2005. Signal role for activation of caspase-3-like protease and burst of superoxide anions during C4+-induced apoptosis of cultured *Taxus cuspidata* cells. Biometals 18, 221–232.
Gerber, I.B., Dubery, I.A., 2003. Fluorescence microplate assay for the detection of oxidative burst products in tobacco cell suspensions using 2′,7′-dichlorofluorescein. Methods in Cell Science: An Official Journal of the Society for In Vitro Biology 25, 115–122.
Gonzalez, P.M., Puntarulo, S., 2011. Iron and nitrosative metabolism in the Antarctic mollusc *Laternula elliptica*. Comparative Biochemistry and Physiology: Toxicology & Pharmacology 153, 243–250.
Graziano, M., Lamattina, L., 2007. Nitric oxide accumulation is required for molecular and physiological responses to iron deficiency in tomato roots. Plant Journal 52, 949–960.

Greenberg, J.T., 1996. Programmed cell death: a way of life for plants. Proceedings of the National Academy of Sciences of the United States of America 93, 12094–12097.
Halliwell, B., 2006. Reactive species and antioxidants. Redox biology is a fundamental theme of aerobic life. Plant Physiology 141, 312–322.
Heath, R.L., Packer, L., 1968. Photoperoxidation in isolated chloroplasts. I. Kinetics and stoechiometry of fatty acid peroxidation. Archives of Biochemistry and Biophysics 125, 189–198.
Houot, V., Etienne, P., Petitot, A.S., Barbier, S., Blein, J.P., Suty, L., 2001. Hydrogen peroxide induces programmed cell death features in cultured tobacco BY-2 cells, in a dose-dependent manner. Journal of Experimental Botany 52, 1721–1730.
Imsande, J., 1998. Iron, sulfur, and chlorophyll deficiencies: a need for an integrative approach in plant physiology. Physiologia Plantarum 103, 139–144.
Iturbe-Ormaetxe, I., Moran, J.F., Arreseigor, C., Gogorcena, Y., Klucas, R.V., Becana, M., 1995. Activated oxygen and antioxidant defenses in iron-deficient pea plants. Plant, Cell & Environment 18, 421–429.
Jeong, J., Guerinot, M.L., 2009. Homing in on iron homeostasis in plants. Trends in Plant Science 14, 280–285.
Jiang, A.L., Cheng, Y.W., Li, J.Y., Zhang, W., 2008. A zinc-dependent nuclear endonuclease is responsible for DNA laddering during salt-induced programmed cell death in root tip cells of rice. Journal of Plant Physiology 165, 1134–1141.
Kempe, D.S., Lang, P.A., Duranton, C., Akel, A., Lang, K.S., Huber, S.M., Wieder, T., Lang, F., 2006. Enhanced programmed cell death of iron-deficient erythrocytes. FASEB Journal 20, 368–370.
Koc, M., Nad'ova, Z., Kovar, J., 2006. Sensitivity of cells to apoptosis induced by iron deprivation can be reversibly changed by iron availability. Cell Proliferation 39, 551–561.
Koch, E., Slusarenko, A., 1990. *Arabidopsis* is susceptible to infection by a downy mildew fungus. Plant Cell 2, 437–445.
Kumar, P., Tewari, R.K., Sharma, P.N., 2010. Sodium nitroprusside-mediated alleviation of iron deficiency and modulation of antioxidant responses in maize plants. AoB Plants 2010, plq002.
Kuthanova, A., Opatrny, Z., Fischer, L., 2008. Is internucleosomal DNA fragmentation an indicator of programmed death in plant cells? Journal of Experimental Botany 59, 2233–2240.
Lam, E., 2008. Programmed cell death in plants: orchestrating an intrinsic suicide program within walls. Critical Reviews in Plant Sciences 27, 413–423.
Law, M.Y., Charles, S.A., Halliwell, B., 1983. Glutathione and ascorbic acid in spinach (*Spinacia oleracea*) chloroplasts – the effect of hydrogen peroxide and paraquat. Biochemical Journal 210, 899–903.
Lichtenthaler, H.K., 1987. Chlorophylls and carotenoids: pigments of photosynthetic biomembranes. In: Packer, L., Douce, R. (Eds.), Plant Cell Membranes. Academic Press Inc., San Diego, pp. 350–382.
Locato, V., Gadaleta, C., De Gara, L., De Pinto, M.C., 2008. Production of reactive species and modulation of antioxidant network in response to heat shock: a critical balance for cell fate. Plant, Cell & Environment 31, 1606–1619.
Maccarrone, M., Van Zadelhoff, G., Veldink, G.A., Vliegenthart, J.F.G., Finazzi-Agro, A., 2000. Early activation of lipoxygenase in lentil (*Lens culinaris*) root protoplasts by oxidative stress induces programmed cell death. European Journal of Biochemistry 267, 5078–5084.
Molassiotis, A., Tanou, G., Diamantidis, G., Patakas, A., Therios, L., 2006. Effects of 4-month Fe deficiency exposure on Fe reduction mechanism, photosynthetic gas exchange, chlorophyll fluorescence and antioxidant defense in two peach rootstocks differing in Fe deficiency tolerance. Journal of Plant Physiology 163, 176–185.
Msilini, N., Attia, H., Bouraoui, N., M'Rah, S., Ksouri, R., Lachaal, M., Ouerghi, Z., 2009. Responses of *Arabidopsis thaliana* to bicarbonate-induced iron deficiency. Acta Physiologiae Plantarum 31, 849–853.
Piszczek, E., Gutman, W., 2007. Caspase-like proteases and their role in programmed cell death in plants. Acta Physiologiae Plantarum 29, 391–398.
Reape, T.J., Molony, E.M., McCabe, P.F., 2008. Programmed cell death in plants: distinguishing between different modes. Journal of Experimental Botany 59, 435–444.
Roschzttardtz, H., Conejero, G., Curie, C., Mari, S., 2010. Straightforward histochemical staining of Fe by the adaptation of an old-school technique: identification of the endodermal vacuole as the site of Fe storage in *Arabidopsis* embryos. Plant Signaling & Behavior 5, 56–57.
Saito, A., Iino, T., Sonoike, K., Miwa, E., Higuchi, K., 2010. Remodeling of the major light-harvesting antenna protein of PSII protects the young leaves of barley (*Hordeum vulgare* L.) from photoinhibition under prolonged iron deficiency. Plant and Cell Physiology 51, 2013–2030.
Simeonova, E., Sikora, A., Charzynska, M., Mostowska, A., 2000. Aspects of programmed cell death during leaf senescence of mono- and dicotyledonous plants. Protoplasma 214, 93–101.
Slesak, I., Libik, M., Karpinska, B., Karpinski, S., Miszalski, Z., 2007. The role of hydrogen peroxide in regulation of plant metabolism and cellular signalling in response to environmental stresses. Acta Biochimica Polonica 54, 39–50.
Suh, Y.A., Arnold, R.S., Lassegue, B., Shi, J., Xu, X.X., Sorescu, D., Chung, A.B., Griendling, K.K., Lambeth, J.D., 1999. Cell transformation by the superoxide-generating oxidase Mox1. Nature 401, 79–82.
Sun, B.T., Jing, Y., Chen, K.M., Song, L.L., Chen, F.J., Zhang, L.X., 2007. Protective effect of nitric oxide on iron deficiency-induced oxidative stress in maize (*Zea mays*). Journal of Plant Physiology 164, 536–543.
Sun, J., Zhang, C.L., Deng, S.R., Lu, C.F., Shen, X., Zhou, X.Y., Zheng, X.J., Hu, Z.M., Chen, S.L., 2012. An ATP signalling pathway in plant cells: extracellular ATP triggers programmed cell death in *Populus euphratica*. Plant, Cell & Environment 35, 893–916.
Tewari, R.K., Kumar, P., Neetu, Sharma, P.N., 2005. Signs of oxidative stress in the chlorotic leaves of iron starved plants. Plant Science 169, 1037–1045.
Tewari, R.K., Kumar, P., Sharma, P.N., 2006. Antioxidant responses to enhanced generation of superoxide anion radical and hydrogen peroxide in the copper-stressed mulberry plants. Planta 223, 1145–1153.
Tewari, R.K., Watanabe, D., Watanabe, M., 2012. Chloroplastic NADPH oxidase-like activity-mediated perpetual hydrogen peroxide generation in the chloroplast induces apoptotic-like death of *Brassica napus* leaf protoplasts. Planta 235, 99–110.
van Doorn, W.G., 2011. Classes of programmed cell death in plants, compared to those in animals. Journal of Experimental Botany 62, 4749–4761.
Watanabe, M., Setoguchi, D., Uehara, K., Ohtsuka, W., Watanabe, Y., 2002. Apoptosis-like cell death of *Brassica napus* leaf protoplasts. New Phytologist 156, 417–426.